INTERNATIONAL JOURNAL OF NUMERICAL MODELLING: ELECTRONIC NETWORKS, DEVICES AND FIELDS
Int. J. Numer. Model. 2010; **23**:266–284
Published online 29 December 2009 in Wiley InterScience (www.interscience.wiley.com). DOI: 10.1002/jnm.737

Atomistic analysis of B clustering and mobility degradation in highly B-doped junctions

Maria Aboy[1,*,†], Lourdes Pelaz[1], Pedro López[1], E. Bruno[2] and S. Mirabella[2]

[1]*Universidad de Valladolid, Campus Miguel Delibes s/n, 47011 Valladolid, Spain*
[2]*MATIS CNR-INFM Via Santa Sofia 64, I-95123 Catania, Italy*

SUMMARY

In this paper we discuss from an atomistic point of view some of the issues involved in the modeling of electrical characteristics evolution in silicon devices as a result of ion implantation and annealing processes in silicon. In particular, evolution of electrically active dose, sheet resistance and hole mobility has been investigated for high B concentration profiles in pre-amorphized Si. For this purpose, Hall measurements combined with atomistic kinetic Monte Carlo atomistic simulations have been performed. An apparent anomalous behavior has been observed for the evolution of the active dose and the sheet resistance, in contrast to opposite trend evolutions reported previously. Our results indicate that this anomalous behavior is due to large variations in hole mobility with active dopant concentration, much larger than that associated to the classical dependence of hole mobility with carrier concentration. Simulations suggest that hole mobility is significantly degraded by the presence of a large concentration of boron-interstitial clusters, indicating the existence of an additional scattering mechanism. Copyright © 2009 John Wiley & Sons, Ltd.

Received 12 June 2009; Revised 15 September 2009; Accepted 29 September 2009

KEY WORDS: process simulation; dopants; defects; diffusion; electrical activation; mobility degradation

1. INTRODUCTION

The shrinking of Si device dimensions has revealed material and process limits that make the fabrication of integrated circuits very complex. In the field of doping technology for planar bulk CMOS devices, one of the most challenging requirements concerns to the achievement of extremely high electrically active doping levels in the source/drain extension regions with ultra-shallow junction depths ($X_j \sim 10\,\text{nm}$) for the control of short-channel effects, while simultaneously minimizing the sheet resistance ($R_S \sim 500\,\Omega/\text{sq}$) and doping abruptness at the extension-channel junction [1].

*Correspondence to: Maria Aboy, Universidad de Valladolid, Campus Miguel Delibes s/n, 47011 Valladolid, Spain.
†E-mail: marabo@tel.uva.es

Contract/grant sponsor: Spanish DGI; contract/grant number: TEC2008-06069

Modeling has become an essential step for the understanding of physical mechanisms involved in junction formation and for process evaluation and optimization. Important and challenging issues in the area of the front-end process modeling are the diffusion and interactions of dopants and defects [1]. These processes are highly transient and its dynamics needs to be captured by models in order to define the optimum processes that provide maximal dopant activation with minimal diffusion. Predictive process simulation has stimulated the development of detailed models about dopant diffusion, evolution of extended defects and formation and dissolution of dopant-defect clusters [2–4]. Although continuum models are the mainstay in process simulators used in the semiconductor industry, atomistic process models are very helpful to extract relevant parameters (diffusivity, binding energies, etc.), to improve the understanding of physical interactions and even to perform full process simulations that can be directly compared to experimental results [3].

We focus on the case of B because it is one of the most common dopants used for the formation of p-type regions due its high solid solubility in Si [5]. B implantation in Si is one of the most prevalent methods to p-type dope semiconductors for junction formation. However, as-implanted ions are usually electrically non-active and the lattice damage deteriorates the device performance [2–4]. A subsequent annealing of the Si substrate is necessary to permit dopant atoms to incorporate into substitutional sites and become electrically active, and to repair the lattice damage. At the same time, undesirable transient enhanced diffusion (TED) and formation of electrically inactive B-Si Interstitial Clusters (BICs) occur, making the formation of ultra-shallow low-resistivity junctions difficult. When B is implanted in crystalline Si, BICs are formed rapidly [3]. Their dissolution requires high thermal budgets and the process is accompanied by significant diffusion, which poses a trade-off between little diffusion and high activation.

It has been reported that pre-amorphizing implants prior to B implantation and followed by solid phase epitaxial regrowth (SPER) reduce the formation of BICs. During low-temperature, SPER damage is swept towards the surface at the same time that most B atoms are incorporated into substitutional lattice sites, resulting in high activation levels ($\sim 10^{20}\,\mathrm{cm}^{-3}$) with minimal diffusion [6, 7]. Higher B concentrations lead to the formation of some BICs in the amorphous region and remain electrically inactive after SPER [6–9]. During post-regrowth annealing, B deactivation and subsequent reactivation, as well as B redistribution, have been reported [6, 7, 10]. As discussed in previous works [9, 10], Si interstitials emitted from end-of-range (EOR) defects (that remain beyond the amorphous/crystalline interface after SPER) interact with the B profile, leading to some growth of preexisting BICs and resulting in the observed B deactivation. Moreover, we have shown recently that even if EOR defects are deep enough to avoid the interaction between EOR defects and the B profile, slight B deactivation also takes place, due to thermally generated equilibrium Si interstitials [11].

The dose of electrically active dopants (N_a) is inversely proportional to R_S and they are related through the hole mobility (μ_p):

$$N_a \approx (q\mu_p R_s)^{-1}\,\mathrm{ohm/sq} \tag{1}$$

Generally, the assessment of the dose of active dopants (N_a) is based on the experimental measurement of R_S, in which it is generally assumed that μ_p only depends on the electrically active dopant concentration [12]. Therefore, the evolution of R_S is commonly understood in terms of the evolution of N_a, showing an inverse trend, whereas changes in μ_p are considered practically negligible in the dopant ranges used in the experiments.

DOI: 10.1002/jnm

In this work we use atomistic simulations to gain physical understanding of the mechanisms associated to B clustering that leads to B deactivation in Si in highly B-doped junctions. Moreover, we present for the first time experimental data combined with kinetic Monte Carlo (KMC) simulations, suggesting that μ_p is largely affected by the amount of BICs.

This paper is organized as follows. In the next section we present a brief revision of different simulation techniques generally used in the study and analysis of physical mechanisms in silicon associated to the fabrication of electronic devices. In particular, the KMC simulation technique used in this work is analyzed in more detail. In Section 3 we describe the experiment we performed to analyze the evolution of N_a, R_S and μ_p in highly B-doped junctions. Later, in Section 4 we present experimental data along with KMC simulations that allow us to analyze and interpret the obtained results. Finally Section 5 is devoted to conclusions.

2. SIMULATION TECHNIQUES FOR THE ANALYSIS OF PROCESSING TECHNOLOGIES IN SILICON DEVICES

Until recently, most of the simulators used for industrial applications were based on the continuum approach. The main reason for taking such an approach was that it was less computationally expensive than any of its atomistic counterparts, and also, they can be more easily coupled to other processes used in the integrated circuit fabrication, such as oxidation, metal deposition, etc. In continuum process simulators or partial differential equation (PDE) solvers, the physics of the system is formulated as a series of differential equations for each particle type. Typically they are continuity equations, where each particle gain or loss is formulated in terms of its generation and recombination rates and the diffusion flux [13, 14]. The reaction rates are defined according to the parameters that characterize their interactions. The numerical solution of these sets of non-linear PDEs requires spatial and temporal discretization to reduce the derivatives into algebraic differences. The problem is converted to a large, nonlinear system of coupled equations, which are solved using standard numerical methods. These simulators are fast and allow the consideration of big sample sizes by adjusting the grid used for the spatial discretization. However, this advantage is reduced as the device size shrinks to nanometric scale. The atomistic nature of the material arises and complex physical interactions show up. The use of a very refined grid and the addition of new equations slow down the resolution of the problem using continuum methods. Then, atomistic simulation techniques, which traditionally have been just used to extract continuum model parameters, become a good alternative even for industrial applications [1, 3, 9–11, 13–15].

2.1. Atomistic simulations

In atomistic simulation techniques the system under study is described taking into account its discrete nature, i.e. as a set of interacting atoms or molecules. Depending on the accuracy used to describe the particle interactions it is possible to distinguish several techniques. The so-called *ab initio* calculations provide an accurate description of the system based on the resolution of the Schrödinger equation for the set of particles (nuclei and electrons) that constitute the system under study. Even though this resolution is carried out using several approximations, this technique provides an accurate description of the interactions based on the electron distribution of the atoms, with no free parameters [16]. However, these methods are computationally very expensive. They can only handle systems of a few hundreds of atoms and are limited to

DOI: 10.1002/jnm

extremely short times, far from the needs of a process simulator. Nevertheless, these methods are useful to calculate the energies of specific atomic configurations and give excellent insight into the appropriate physics [17]. For example, *ab initio* methods were used to provide a detailed insight into the physics associated to the mechanism of B diffusion [18].

Classical molecular dynamics (MD) simulations describe the atomic interactions by empirical force laws. The parameters that describe the empirical interatomic potentials are chosen by fitting to experimental data or *ab initio* calculations [19, 20]. By this technique it is possible to simulate systems containing thousands of atoms for times of the order of nanoseconds, but at the expense of losing the electronic description of the system. MD simulations reproduce the actual dynamics of all system atoms and thus it is possible to determine diffusion paths, evolution among different atomic defect configurations [21], and even the damage caused by an energetic ion colliding with a Si lattice [22]. For example, MD simulations have been very useful in the study of the stability of the so-called 'bond-defect' or interstitial-vacancy pair, and its relevance in the amorphization of silicon [23]. However, it is not feasible to simulate the complete implantation and subsequent annealing, as these processes involve times in the order of seconds or even minutes.

Simulation methods considered so far allow a full description of the system dynamics at the atomic level. However, the time and size scales accessible to them are still orders of magnitude far from experimental conditions. In other words, when process that handles particles with energies that vary several orders of magnitude needs to be simulated, as it occurs for example in the case of ion implantation, previous methods are inappropriate. There are several alternative methods that maintain the atomic level description, but in order to reach experimental sizes and times they must renounce to keep the full dynamics of the system. In the binary collision approximation (BCA) the implantation process is simulated by calculating collisions between ions or Si recoils and the Si target atoms by assuming that the energetic atom interacts only with the closest atom in its neighborhood [24]. Target atoms can be part of a crystalline structure or a material without any structure (amorphous). The codes MARLOWE [24] and TRIM [25] have been developed for crystalline and amorphous materials, respectively. BCA methods provide the atomic coordinates of the implanted ion and the generated Si interstitials and vacancies during the collision cascade. Thousands of cascades can be easily calculated to provide enough statistical resolution and generate reliable dopant and damage profiles. Ideally, a reduced number of parameters should be enough to describe the nuclear and electronic interactions in the collision of any ion-target atom combination [26]. However, an extended number of model parameters are frequently used to get better fit to experimental results.

On the other hand, KMC codes allow the simulation of the annealing step by only handling dopant atoms and lattice defects and their interactions [1, 3, 9–11, 13–15]. Parameters that define these interactions, such as diffusivities, binding energies, capture radius, etc., must be specified. These parameters are derived from *ab initio* [18, 27–30] and MD [22, 23] calculations, or dedicated experiments [3, 4, 31]. In lattice KMC codes, all the atoms in the lattice are included in the simulation [32]. On the contrary, in non-lattice KMC codes, only the intrinsic (Si interstitial and vacancies) and extrinsic (dopants and impurities) defects are included in the simulation [15]. Therefore, unlike MD simulations, the vibrational movement of the Si lattice atoms is not simulated, and only the dynamics of the defects and the dopants (diffusion, emission from clusters, recombination…) is followed. This allows the simulation of systems of hundreds of nanometers, and thus, current devices are accessible to this technique. Moreover, this lets a variable simulation time-step during the simulation, which may go from 10^{-9} s for

DOI: 10.1002/jnm

some diffusing species to 10^3 s, or even longer, for the emission of defects from stable clusters. Generally, the fastest events tend to disappear quickly leaving slower events that raise the time-step. This allows to easily access to macroscopic times, and so to the simulation of actual processing. Therefore, their results can be directly compared to experimental results, being a good alternative to continuum process simulators as the device size shrinks, even for industrial applications.

2.2. Modeling of defects, dopants and their interactions in non-lattice KMC methods

Our work is focused on the ion implantation and annealing processes, and thus, a comprehensive analysis and understanding of the phenomenon of diffusion of point defects and dopants, as well as the possible interactions among them is necessary. Theoretical calculations, combined with focused experiments, have led to the improved physical understanding of dopant implantation, diffusion and activation. Ion implantation of dopants generates large amounts of Frenkel pairs. During the annealing, Si interstitials and vacancies recombine or form clusters and extended defects [33]. The presence of these defects significantly alters dopant diffusion [2, 34]. Complex reactions between dopant and defects may cause dopant clustering and electrical deactivation [2–4]. All these mechanisms need to be included in process simulators to give them the capability of predicting the electrically active dopant distribution, resulting from ion implantation and annealing processes.

In KMC methods, chemical reactions used in continuum simulators are associated to particle interactions and events, and each particle is traced individually. As an example, we will consider the Si interstitial diffusion and the interactions among interstitials to evolve into agglomerates. Theoretical calculations indicate that there is a strong, energetic driving force favoring the clustering of individual interstitials into dimmers and for further growth into large clusters [22]. This has been confirmed by the experimental observation of extended Si interstitial agglomerates, such as 'rod-like' defects known as {113} defects [34] and dislocation loops [35]. The modeling of the Si interstitial clustering evolution can be written as a chemical reaction between a mobile-free interstitial, I, and an interstitial cluster with n_{CI} interstitials, $C_{(n\mathrm{CI})}$, to result in an interstitial cluster with $n_{\mathrm{CI}}+1$ interstitials, $C_{(n\mathrm{CI}+1)}$

$$I + C_{(n\mathrm{CI})} \leftrightarrow C_{(n\mathrm{CI}+1)}. \tag{2}$$

In this example, a Si interstitial in a cluster can be emitted (event) or can interact with a free Si interstitial and capture it (interaction). A free Si interstitial can experience diffusion hops (event) or interact with an interstitial cluster and be captured. Events are characterized by the emission or jump frequencies, and interactions are characterized by a capture radius. The total event rate, R, of a system with n_{I} free Si interstitials and n_{CI} Si interstitials in clusters is

$$R = R_{\mathrm{I\ migration}} + R_{\mathrm{I\ emission\ from\ cluster}} = n_{\mathrm{I}} \frac{6D_{\mathrm{I}}}{(\beta a)^2} + n_{\mathrm{CI}} \frac{6D_{\mathrm{I}}}{(\beta a)^2} \exp\left(-\frac{E^I_{\mathrm{bind}}}{k_{\mathrm{B}}T}\right) \tag{3}$$

where $E^{\mathrm{I}}_{\mathrm{bind}}$ is the binding energy of the Si interstitial to the cluster, βa the hop distance in terms of the silicon lattice spacing (a), k_{B} the Boltzmann constant, T the absolute temperature and D_{I} the Si interstitial diffusivity, which can be expressed as

$$D_{\mathrm{I}} = \frac{(\beta a)^2}{6} \nu_0 \exp\left(-\frac{S^{\mathrm{I}}_{\mathrm{m}}}{k_{\mathrm{B}}}\right) \exp\left(-\frac{E^{\mathrm{I}}_{\mathrm{m}}}{k_{\mathrm{B}}T}\right) = \nu^{\mathrm{m}}_{0\mathrm{I}} \exp\left(-\frac{E^{\mathrm{I}}_{\mathrm{m}}}{k_{\mathrm{B}}T}\right) \tag{4}$$

DOI: 10.1002/jnm

where v_0 is the vibrational frequency of an atom in the Si lattice, S_m^I and E_m^I the migrational entrophy and enthalpy respectively, and v_{0I}^m represents a prefactor for Si interstitial migration, which includes all constant values and leads to a more simplified expression. Thus, Equation (3) for the total event rate, R, of a system with n_I free Si interstitials and n_{CI} Si interstitials in clusters can be reformulated as

$$R = n_I v_{0I}^m \exp\left(-\frac{E_m^I}{k_B T}\right) + n_{CI} v_{0CI}^b \exp\left(-\frac{E_m^I + E_{bind}^I}{k_B T}\right) \tag{5}$$

where v_{0CI}^b represents a prefactor for interstitial emission from an interstitial cluster.

Once the total event rate of the system is established, the basic scheme for each simulation step is shown schematically in Figure 1 and can be explained as follows. A random number ($0 < \mathrm{rn1} < R$) determines the event: a diffusion hop or the interstitial emission from a cluster. Depending on the selected event, another random number ($0 < \mathrm{rn2} < n_I$, or $0 < \mathrm{rn2} < n_{CI}$) chooses the particular interstitial that experiences the event. An additional random number gives the direction of the jump (or emission) to a distance βa. When the selected particle is moved to a new position, its neighbors are checked for possible interactions. The neighbors are defined as particles that lie within the capture radius, αa, of a given particle. If, for instance, a free interstitial experiences a diffusion hop and lies within the capture radius of an interstitial cluster, the free interstitial disappears and becomes part of the cluster. Then, the total event rate must be updated to

$$R = (n_I - 1)\frac{6D_I}{(\beta a)^2} + (n_{CI} + 1)\frac{6D_I}{(\beta a)^2} \exp\left(-\frac{E_{bind}^I}{k_B T}\right) \tag{6}$$

The simulation of an event increases the time by an amount $\Delta t = 1/R$ and the scheme is repeated until the specified time is reached. The time step is mostly determined by the faster event. The frequency associated to diffusion events is many orders of magnitude higher than that associated to the emission of interstitials from clusters. For example, at 800°C, if we take $D_I = 10^{-6}\,\mathrm{cm}^2/\mathrm{s}$, $\beta a = 3.84\,\text{Å}$ and $E_{bind}^I = 2.6\,\mathrm{eV}$, the diffusion frequency is $\sim 10^9\,\mathrm{s}^{-1}$, while the emission frequency is 12 orders of magnitude slower, as it is shown schematically in Figure 2. The time step for each diffusion event is very small ($< 10^{-9}\,\mathrm{s}$) and a huge amount ($> 10^9$) of these events should be simulated for the time to advance one second. On average, the faster event will be selected orders of magnitude more often than the slower event. This means that

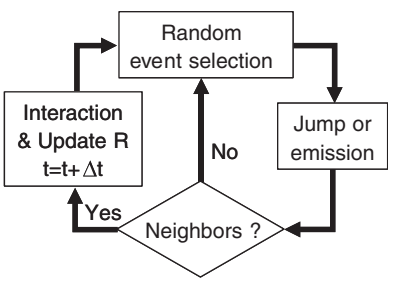

Figure 1. Basic scheme of simulation steps in kMC methods. A random number determines the event. An additional random number gives the direction of the jump (or emission) to a distance βa. Once the selected particle is moved to a new position, its neighbors (particles that lie within the capture radius, αa) are checked for possible interactions. Then, the simulation time increases an amount $\Delta t = 1/R$ and the scheme is repeated until the specified time is reached.

DOI: 10.1002/jnm

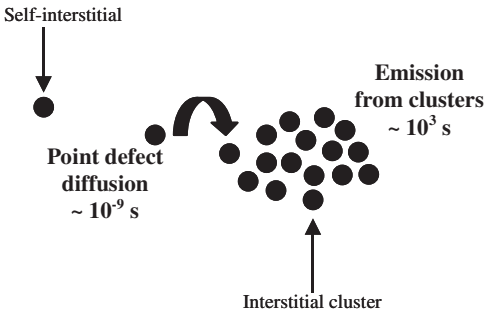

Figure 2. During the simulation the simulation time-step may go from 10^{-9} s for some diffusing species, such as Si interstitial diffusion, to 10^3 s, or even longer, for the emission of defects from stable clusters, such us Si interstitial emission from interstitial clusters.

free interstitials are very likely to be selected, experience diffusion hops and be captured before any of the interstitials in clusters are emitted. The system thus ends up with (n_I+n_{CI}) interstitials trapped in clusters. In that instant, the emission of an interstitial from a cluster is the only possible event, which gives a time step 12 orders of magnitude higher than that associated with diffusion events. This increase in the time step makes the simulation of actual process times possible. Since particles are chosen randomly according to their event rates, a large number of particles must be included in the simulation cell to reduce the statistical error. However, with the computer power available nowadays, hundreds of thousands of particles can be easily traced.

Continuing with the same example, the rate of change of the clustered Si interstitial concentration, C_C (Equation (7)), and that of the free Si interstitial concentration, C_I (Equation (8)), can be formulated as a PDE in terms of the Si interstitial cluster growth and dissolution rates through the capture and emission of free interstitials [33, 36]:

$$\frac{\partial C_C}{\partial t} = 4\pi\frac{(\alpha a)^3}{(\beta a)^2}\cdot D_I\cdot C_C\cdot C_I - \frac{6D_I}{(\beta a)^2}\exp\left(-\frac{E^I_{bind}}{k_B T}\right)\cdot C_C \tag{7}$$

$$\frac{\partial C_I}{\partial t} = \nabla(D_I\cdot\nabla C_I) - 4\pi\frac{(\alpha a)^3}{(\beta a)^2}\cdot D_I\cdot C_C\cdot C_I + \frac{6D_I}{(\beta a)^2}\exp\left(-\frac{E^I_{bind}}{k_B T}\right)\cdot C_C \tag{8}$$

where *áa* represents the capture radius in terms of the silicon lattice spacing. The cluster growth rate depends on the amount of clusters and interstitials, the capture volume and the jump frequency of the interstitial whereas the cluster dissolution rate depends on the amount of clusters and on the rate of emission of the interstitial from the clusters (bounded to the clusters by an energy E^I_{bind}). The equation for free Si interstitials (Equation (8)) also includes the gradient of the flux, as free interstitials are mobile.

New particles and new events and interactions can be easily added in the model. If other defects such as vacancies, dopants or traps were considered, similar equations to those for Si interstitials should be formulated for each of them. In addition, coupling terms corresponding to interstitial–vacancy or dopant–interstitial interactions should be added to the differential equations, which make their resolution more difficult. In KMC methods, additional reactions only require new event rates to be added to the total event rate, and the proper definition of the capture radius of the interactions. As an example, if we also consider boron diffusion, we should include a chemical reaction between a Si interstitial, I, and a substitutional boron atom, B_s, to

DOI: 10.1002/jnm

result in a mobile interstitial–boron pair, B_i, since it is known that B mainly diffuse through Si interstitials [18, 27, 28].

$$I + B_s \leftrightarrow B_i. \tag{9}$$

In KMC this new interaction is modeled with two new event rates, one related to B_i diffusion (third term in Equation (10)), and the other related to B_i breakup (fourth term in Equation (10))

$$\begin{aligned} R = & n_I \nu_{0I}^{m} \exp\left(-\frac{E_m^I}{k_B T}\right) + n_{CI} \nu_{0CI}^{b} \exp\left(-\frac{E_m^I + E_{bind}^I}{k_B T}\right) \\ & + n_{Bi} \nu_{0Bi}^{m} \exp\left(-\frac{E_m^{Bi}}{k_B T}\right) + n_{Bi} \nu_{0Bi}^{break} \exp\left(-\frac{E_{bind}^{Bi} + E_m^I}{k_B T}\right) \end{aligned} \tag{10}$$

where ν_{0Bi}^{m} and ν_{0Bi}^{break} are prefactors for B_i migration and B_i breakup, respectively. Thus, new reactions only add new event rates to the total event rate and this addition hardly adds any computational load. The main difficulty arises from the determination of the new parameters (binding energies, diffusivities, capture radius…) that describe the interactions, but this is also necessary in continuum methods.

2.3. Simulation scheme and basic parameters for defects and dopants used in the non-lattice KMC code DADOS

The main tool we use for the analysis of defect and dopants interactions is a non-lattice KMC code developed in the department of Electronics of the University of Valladolid, DADOS (Diffusion of Atomistic Defects, Object-Oriented Simulator), which describes diffusion events and interactions between defects and dopants in silicon [15]. In Figure 3 is shown schematically the structure of our simulations.

To simulate the implantation cascades we use a code based in the BCA, which is called MARLOWE [24]. This code generates the coordinates of the implanted ions along with the displaced atoms in each implantation cascade. These coordinates of dopants, Si interstitials and

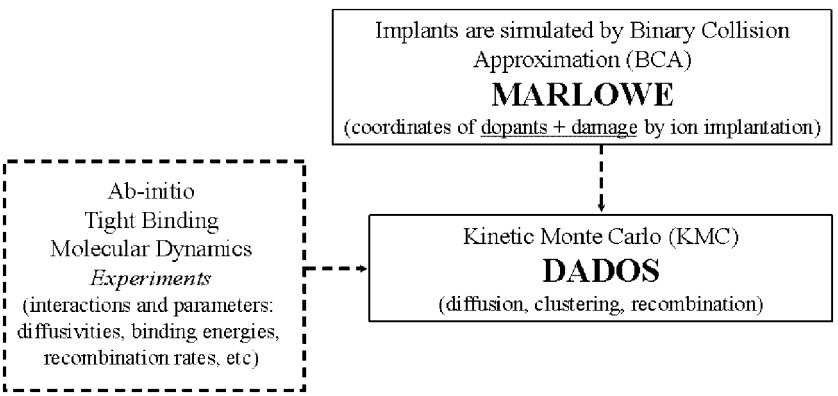

Figure 3. Schematic of the structure of simulations in the non-lattice kMC code DADOS. The implantation cascades are simulated with the code MARLOWE, which generates the coordinates of the implanted dopants and the resulting damage. These coordinates are transferred to DADOS in order to simulate their evolution during ion implantation and subsequent annealing. The parameters that define the interactions are extracted from theoretical calculations or dedicated experiments.

DOI: 10.1002/jnm

vacancies are transferred to the non-lattice KMC code, DADOS, to simulate the evolution of these dopants and damage during ion implantation and post-implant annealing. In this KMC code, only the atoms belonging to point or extended defects are simulated. Clusters of point defects are formed when the mobile point defects jump within the capture radius of other point defects or pre-existing clusters. We consider that defects interact when they are within second-neighbor distance (3.84 Å) of each other. Defects experience diffusion or emission events at a rate determined by their binding energy. Thus, the KMC method is an event-driven technique, i.e. simulates events at random with probabilities according to the corresponding event rates. In this way it self-adjusts the time-step as the simulation proceeds, depending on the fastest event present at that time. The time-step can, in fact, change automatically from picoseconds to hours and back to nanoseconds, depending on the defects present as the simulation evolves. The sequencing of events and the calculation of the time elapsed between two consecutive events is done based on the current defect configuration.

The binding energies used in our non-lattice KMC simulations are obtained from *ab initio* calculations or dedicated experiments, or estimated by inverse modeling over experimental data. Main parameters used in our simulations are specified below.

The formation and migration energies of the free Si self-interstitial and vacancy are taken from Reference [31]. Si interstitials and vacancies can condense into agglomerates of Si interstitials and vacancies, respectively. In the case of Si interstitials, these agglomerates can be small clusters, {113} defects or dislocation loops, while in the case of vacancies, they are agglomerates or clusters of vacancies. For small Si interstitial clusters we take the oscillating formation energies experimentally deduced by Cowern *et al*. [33]. For Si interstitial defects with larger sizes, we use the experimental binding energy of {113} defects [33] and dislocation loops [35]. For vacancy clusters we take the oscillating formation energies reported by Bongiorno *et al*. [37]. The surface is considered as an efficient sink for point defects.

Concerning to dopant modeling, we consider that boron diffuses by an interstitialcy mechanism [18], based in B diffusion through a mobile B_i pair with migration and binding energies taken from References [18, 28]. The precipitation and immobilization of B atoms has been associated to the formation of electrically inactive BICs [2–4, 9, 29, 30]. In our model, these BICs consist of B_nI_m complexes with n B atoms and m Si interstitials [3, 4, 9]. Although there are some discrepancies about specific energy values for different B_nI_m configurations [3, 4, 29, 30], experimental observations and theoretical calculations indicate that configurations with no Si interstitials are energetically unfavorable and the presence of Si interstitials reduces the energy of the BICs. Based on those observations and calculations, we have developed a B clustering model that includes a complex pathway for B/Si interstitial interactions [3, 4, 9]. Total energies of the B_nI_m complexes with $n \leqslant 4$ are given by the expression reported in Reference [4],] which is consistent with other proposed models [3, 29, 30]. BICs with no Si interstitials (B_2, B_3 and B_4) have positive total energy in the model [9], according to theoretical calculations [29]. Since we consider the free components as the energy reference level, BICs with no Si interstitials are unstable. Adding Si interstitials, the stability of the BICs is increased, at least up to about 4–5 Si interstitials per cluster [38]. Classical models for B clustering included complexes of B atoms and Si interstitials, B_nI_m, that contain only few atoms, up to 4 B atoms and 4 interstitial defects generally [3, 4, 9, 29, 30]. However, recent experiments have evidenced the formation of larger and very stable BICs, which are observed only under conditions of very high B concentrations [39, 40]. Experiments indicate that their contribution to B deactivation becomes very significant at B concentrations higher than $\sim 10^{20}\,\mathrm{cm}^{-3}$. Because of the very high B concentrations present

DOI: 10.1002/jnm

in the experiments under study, we have considered a new extended model for BICs that we have developed recently [11], which considers larger and more stable BICs than those included in classical models. Based on experimental evidences [39, 40] we proposed the existence of two different species of BICs: the classical small ($n \leqslant 4$) and less stable BICs explained above and a new type of larger and more stable BICs that only form in the presence of very high B concentrations. Since these large BICs have been observed only in the presence of very high B concentrations (well above equilibrium solid solubility) we propose that B_5I_m configurations have high potential energy, with negative binding energy. Otherwise, small BICs tend to grow into large configurations even in the presence of low B concentrations, contrary to experimental evidences. This extended model is consistent with previous studies for low and middle B concentrations under very different experimental conditions [9]. Only in the presence of very high B concentrations, BICs could evolve towards B_nI_m configurations with $n > 5$, which have again low potential energy in the model according to experimental suggestions [39, 40]. Furthermore, the activation energy for the emission of mobile B_i from these large configurations ($n > 5$) is higher than for usual small configurations (up to $n = 4$). Thus, for large configurations we establish an activation energy for the emission of B_i from stable configurations around 4.5 eV [39] whereas for usual small BICs was around 3.7 eV [38, 39]. This causes a slower dissolution rate when larger BICs are formed at high B concentrations.

3. EXPERIMENTAL

The main objective of this work is the analysis of the evolution of N_a, R_S and μ_p for high concentration ($> 10^{21}\,cm^{-3}$) B profiles in pre-amorphized Si during different annealing after SPER. For this purpose, experiments have been performed on *n*-type, Si Czochralski (100) wafers (resistivity 1.5–4 Ω cm). Pre-amorphization implant was performed at liquid nitrogen (LN_2) temperature with 500 keV, $5 \times 10^{15}\,cm^{-2}$ plus 40 keV, $1 \times 10^{15}\,cm^{-2}$ Si^- ion beams, obtaining a full amorphous *a*-layer from the surface down to ~950 nm. B implantation at 26 keV, $2 \times 10^{16}\,cm^{-2}$ was performed resulting in a B profile with a maximum concentration of $2 \times 10^{21}\,cm^{-3}$ at the depth of ~120 nm [41]. Implanted B profile and *p-n* junction are entirely contained within 250 nm from the surface. Then, rapid thermal annealing for 30 s at 700°C was performed under N_2 flux to induce fully recrystallization of the pre-amorphized layer. To investigate the evolution of the active B dose and BICs during annealing as a function of time after SPER, we annealed the samples at 850 or 1000°C for times ranging from 1 to 10 000 s. Hall effect was used to determine the Hall active dose (N_H). These measurements are affected by an error of about 5%. The active B dose (N_a) was computed as $N_a = N_H \times r_H$, where r_H is the Hall scattering factor (0.75 for Si [42]).

4. RESULTS AND DISCUSSION

To investigate the evolution of the electrically active B dose during annealing after SPER, we have compared experimental data with our KMC simulations. Although detailed atomistic models that capture the kinetics of the amorphization process have been reported [43], a simple and commonly used amorphization model considers that a damaged region turns amorphous when a critical defect concentration is reached [44]. There are experimental evidences indicating that defects from pre-amorphizing implants contained within the amorphous region are swept towards the surface as SPER takes place [45]. Thus, only the damage beyond the amorphous/crystalline interface remains after the recrystallization process. The interactions of dopants in

DOI: 10.1002/jnm

amorphous Si are not clearly defined, but experiments indicate that the maximum electrically activated B concentration is $\sim 2 \times 10^{20}\,\mathrm{cm}^{-3}$ after SPER [6, 7]. Therefore, in terms of modeling, B atoms are incorporated into substitutional positions at the same time that Si atoms are rearranged layer by layer as SPER proceeds. However, when a high B concentration is present in the pre-amorphized layer, B activation is not complete during SPER. Experiments [6, 7] and theoretical calculations [8] seem to evidence B clustering within the regrown layer for high B concentrations. Sheet resistance measurements [6, 7] and the hump observed in Secondary Ion Mass Spectrometry (SIMS) profiles (associated to B diffusion in amorphous Si) [6, 7] are consistent with active B concentrations up to a few times $10^{20}\,\mathrm{cm}^{-3}$ for regrowth temperatures around 600°C, and higher levels can be reached if the regrowth takes place at higher temperatures [46]. The study of the formation of BICs in amorphous Si requires a complex modeling. However, using the described model of critical defect concentration, and assuming the formation of stable BIC configurations during SPER, we could study the evolution of these BICs upon subsequent annealing. Figure 4 shows the simulated implanted B profile (at 26 keV, $2 \times 10^{16}\,\mathrm{cm}^{-2}$, similarly to experiments) and the position of the residual Si interstitial EOR defects band that remains after SPER (experimentally observed by transmission electron microscopy (TEM) analysis, not shown in the article). Because of the uncertainty that still exists about the initial conditions for B atoms after SPER processes and based on the previous discussion, for our simulations we use the simulated implanted B profile as initial condition. For this B profile we assume that only B concentrations up to a maximum value $[B_{act}]^{max} \sim 2 \times 10^{20}\,\mathrm{cm}^{-3}$ are incorporated into substitutional positions (i.e. are electrically active) after the regrowth, according to experimental data [6, 7]. Moreover, we consider that B concentrations above that value are in the form of small BICs, in agreement with theoretical calculations [8] and previous work [9–11]. Although there is still no agreement on the particular configurations of

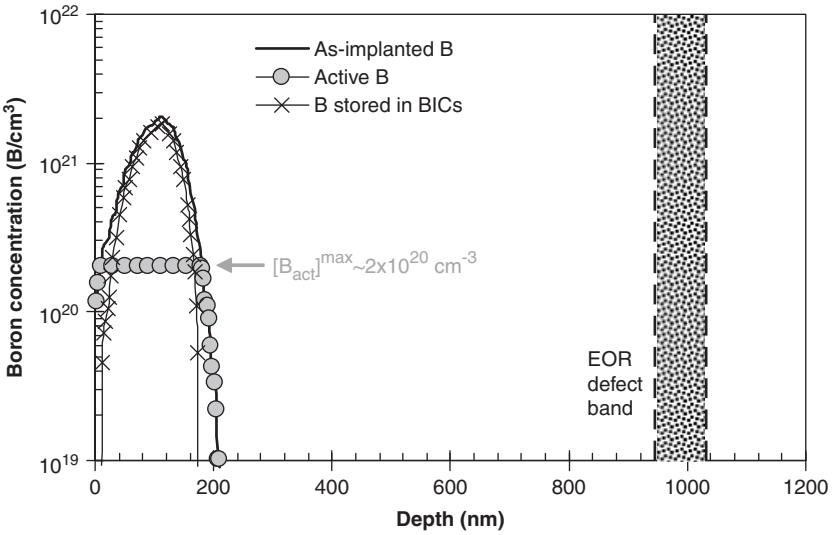

Figure 4. Simulated B concentration profile for B implanted at 26 keV, $2 \times 10^{16}\,\mathrm{cm}^{-2}$. After SPER, B concentrations up to $[B_{act}]^{max} \sim 2 \times 10^{20}\,\mathrm{cm}^{-3}$ are considered electrically active [2, 3] whereas B concentrations above that value are stored in small BICs [2–8]. The position of the residual Si interstitial EOR defects band that remains after SPER is included schematically.

DOI: 10.1002/jnm

BICs that result after SPER, several studies indicate that resulting BICs should be poor in Si interstitials [8–11]. Since SPER removes Si interstitials in the pre-amorphized region, the formation of BICs with Si interstitials would require the formation of extra Si interstitials [11, 47]. According to our B clustering model, the most energetically favorable configurations for BICs are B_2, B_3, B_4, B_3I and B_4I. Larger configurations such us B_6, B_7, B_6I, B_7I, B_7I_2, etc. are also energetically favorable, although the probability of growing into such large BICs becomes lower at these B concentrations. Based on these features, we have considered that, at these relatively high B concentrations, BICs after SPER are mainly in the form of B_4I_m ($\sim$75%), B_3I_m ($\sim$20%), B_6I_m ($\sim$5%) with $m \leqslant 1$. These conditions lead to the best fitting between simulations and experimental data.

Figure 5 shows the time evolution of experimental N_a and R_S values (extracted from Hall measurements) during annealing at (a) 850°C and (b) 1000°C after SPER. Simulation results for N_a are also included, showing a good agreement with the experimental data. Results for the evolution on N_a show that during annealing at 850°C (Figure 5(a)) B slowly deactivates. This B deactivation is mainly controlled by thermally generated Si interstitials, since EOR defects are far enough (at $\sim$950 nm) to avoid their interaction with the B profile (projected range at $\sim$120 nm). Moreover, in order to ensure that EOR defects do not interact with the B profile, reference experiments (not shown in this article) with a 50 nm-wide $Si_{1-y}C_y$ layer ($y = 0.3$ at.%) at a depth of 450 nm (which acts as a trap for Si interstitials) were also performed. Experimental results with and without the $Si_{1-y}C_y$ were practically the same. Simulations also show that the main mechanisms for B deactivation are the interaction of equilibrium interstitials with electrically active B atoms to form mobile B_i pairs that at the same time are able to interact with preexisting BICs by reactions

$$B_nI_m + B_i \leftrightarrow B_{n+1}I_{m+1} \tag{11}$$

Since the transport capability of equilibrium Si self-interstitials has a high activation energy [31] (formation energy+migration energy), only a small fraction of B atoms deactivates and it occurs at a slow rate. Nevertheless, if formed B_nI_m configurations contain more than one Si interstitial these configurations tend to emit a Si interstitial quickly to reach configurations such us B_nI, since they are more stable in the model. Thus, once equilibrium Si interstitials start deactivation reactions, extra Si interstitials contained in the initial BICs will be liberated and available to interact with other BICs. These extra Si interstitials, contained initially in the starting configurations of BICs, accelerates the deactivation process. On the other hand, during annealing at 1000°C (Figure 2(b)), B slightly reactivates at the beginning of the annealing, due to the faster dissolution rate of small BICs compared to their formation rate at high temperatures [10]. However, at long time annealing some B deactivation is again observed. Simulations indicate that the observed B deactivation at long time annealing is due to the evolution of a fraction of small BICs (such us B_4) towards larger and more stable configurations (such us B_6I, B_7I, etc.) that are able to form in the presence of such a high B concentration after intense thermal budgets. This fact has also been experimentally confirmed by weak beam dark field TEM analysis [48].

An interesting feature that reveals experimental data included on Figure 5 is the apparent 'anomalous' behavior of R_S and N_a at long time annealing. Experimental data indicate that R_S and N_a initially evolve with opposite trends, as it has been generally assumed. However, at long time annealing, an 'anomalous' behavior (marked with ovals in Figure 5) is observed. At long time annealing at 850°C (Figure 5(a)) R_S decreases and at long time annealing at 1000°C (Figure 5(b))

DOI: 10.1002/jnm

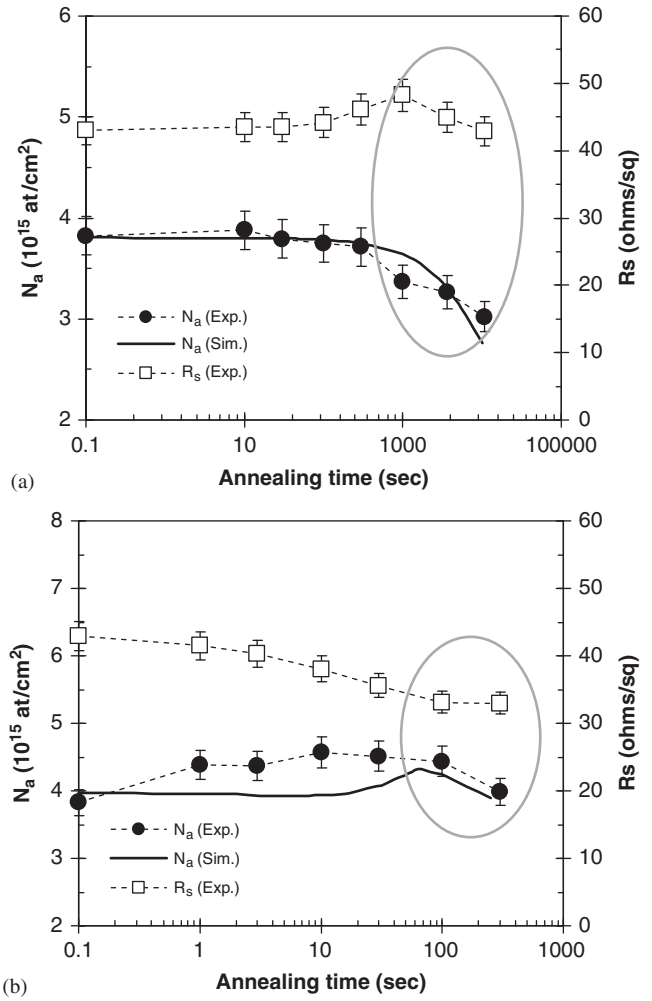

Figure 5. Time evolution of experimental R_S and N_a values (extracted from Hall measurements) during annealing at (a) 850°C and (b) 1000°C after recrystallization. Simulation results for N_a are also included, showing a good agreement with experiments. Results indicate that R_S and N_a initially evolve with opposite trends, as it has been generally assumed. However, at long time annealing an 'anomalous' behavior (marked with ovals) is observed, since N_a decreases (a–b) at the same time that R_S also decreases (a) or remains approximately constant (b), contrary to expected.

R_S remains approximately constant (1000°C), and at the same time N_a also decreases in both situations, contrary to expected.

In an attempt to find a possible explanation for this 'anomalous' behavior we have investigated the evolution of μ_p during annealing, since it also may affect the evolution of R_S. Generally, it is assumed that μ_p is mostly dependent on the carrier concentration [12]. In order to analyze the evolution of active B concentration during annealing at 850 and 1000°C, we could estimate the maximum active B concentration level ($[B_{act}]^{max}$) that corresponds to each measured N_a value during annealing. By assuming a negligible B diffusion during annealing (B

DOI: 10.1002/jnm

diffusion length is in the order of 10–15 nm after 850°C 10 000 s annealing and it is approximately 20–25 nm after 1000°C, 300 s annealing [18, 28]), we could obtain N_a by integrating the as-implanted B profile below a certain $[B_{act}]^{max}$ value (see Figure 4). Even if some B diffusion had occurred, the B profile would become broader and with lower $[B_{act}]^{max}$. This potentially overestimates the $[B_{act}]^{max}$ at longer times. The estimated values for $[B_{act}]^{max}$ for different annealing times at both temperatures are included in Table I. We have also included the estimated hole mobility values predicted by the expression reported by Massetti *et al.* ($\mu_p^{Masetti}$) [12], which assumes that hole mobility depends only on active B concentration. As it is shown in Table I, in the 850°C annealing $[B_{act}]^{max}$ varies approximately between 2.09×10^{20} and $1.59 \times 10^{20}\,cm^{-3}$. According to Masetti *et al.* $\mu_p^{Masetti}$ should vary between 45.5 and 47.4 cm^2/Vs. During the 1000°C annealing $[B_{act}]^{max}$ varies between 2.5×10^{20} and $2.16 \times 10^{20}\,cm^{-3}$, and thus, $\mu_p^{Masetti}$ should vary between 44 and 45.6 cm^2/Vs. Therefore, in both situations the hole mobility should experience very small variations during annealing, according to the behavior generally assumed. The systematically slight overestimation of $[B_{act}]^{max}$ at long annealing times (at which B diffusion is not negligible) leads us to slightly underestimated values for $\mu_p^{Masetti}$.

Nevertheless, experiments reveal a significantly different behavior for μ_p. Figure 6 plots the time evolution of experimental μ_p (extracted from Hall measurements) during annealing at (a) 850°C and (b) 1000°C after SPER. For comparison, the expected estimated range of variation of $\mu_p^{Masetti}$ (see Table I) is also marked schematically in the figure. In spite the estimated values predict changes in $\mu_p^{Masetti}$ lower than 5% during both annealing, experiments show a significant μ_p increase ($\sim$30%) at long time annealing. This high increase in μ_p observed at long time annealing is responsible of the 'anomalous' behavior observed in Figure 5. Moreover, at short annealing times, the μ_p measured is significantly lower than expected from Masetti *et al.* and at long time annealing more agreement between experimental and expected hole mobility is observed. These results suggest that some additional scattering centers that largely degrade μ_p may exist at short time annealing, whereas at long time annealing their effect in μ_p would become practically negligible. In order to find a possible source for the observed mobility degradation we have included in Figure 6 the time evolution of the simulated dose of BICs obtained during annealing at (a) 850°C and (b) 1000°C. Simulations show that the amount of BICs is almost constant at the initial stages of the annealing, and it rapidly decreases at long time annealing. These results suggest that initially the large amount of BICs may act as additional scattering centers with respect to ionized dopants and phonons, lowering μ_p at levels

Table I. Estimated values for $[B_{act}]^{max}$ and μ_p (deduced by the expression reported by Masetti *et al.* [12]) for different instants during 850 and 1000°C anneals.

850°C			1000°C		
Time (s)	$[B_{act}]^{max}$ (cm^{-3})	$\mu_p^{Masetti}$ (cm^2/Vs)	Time (s)	$[B_{act}]^{max}$ (cm^{-3})	$\mu_p^{Masetti}$ (cm^2/Vs)
0.1	2.07×10^{20}	45.6	0.1	2.07×10^{20}	45.6
10	2.09×10^{20}	45.5	1	2.40×10^{20}	44.4
30	2.04×10^{20}	45.7	3	2.37×10^{20}	44.5
100	2.03×10^{20}	45.7	10	2.50×10^{20}	44.0
300	1.99×10^{20}	45.9	30	2.47×10^{20}	44.1
1000	1.80×10^{20}	46.6	100	2.52×10^{20}	44.3
3600	1.73×10^{20}	46.8	300	2.16×10^{20}	45.2
10 800	1.59×10^{20}	47.4			

DOI: 10.1002/jnm

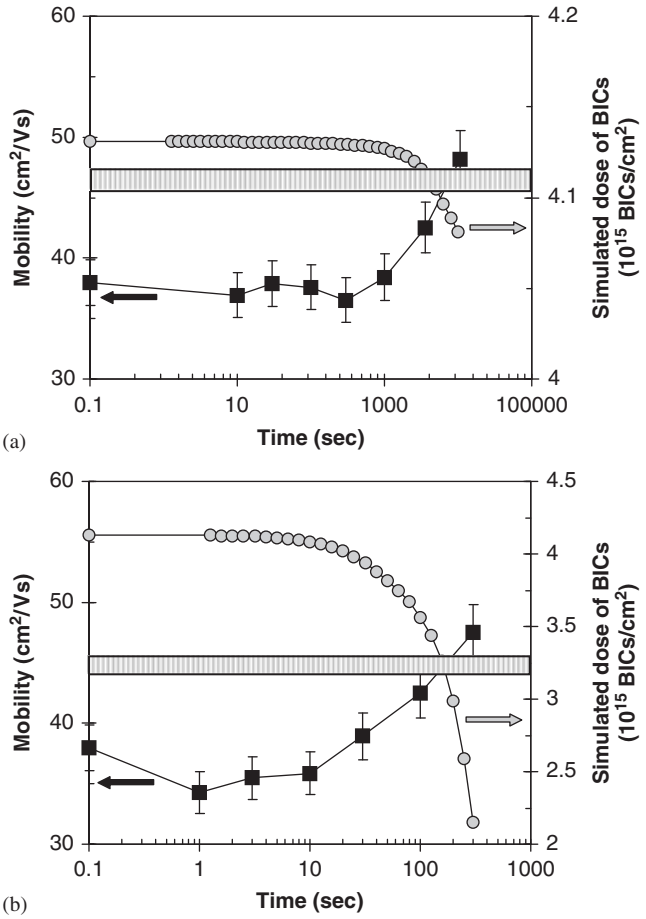

Figure 6. Time evolution of experimental hole mobility μ_p) (extracted from Hall measurements) during annealing at (a) 850°C and (b) 1000°C after SPER. The significant high increase in μ_p observed at long time annealing is responsible of the 'anomalous' behavior observed in Figure 2. We also include the simulated time evolution of the dose of BICs during annealing. A correlation between the high increase in μ_p and the high decrease in the amount of BICs is observed. This suggests that μ_p could be decreased by the presence of a large amount of BICs, since they could act as additional scattering centers.

even smaller than the values predicted by Masetti *et al*. [12]. During annealing, the total amount of BICs decreases (through evolution to larger sizes or through dissolution of small BICs) and μ_p is significantly modified in such a way that variations in μ_p largely affect the R_S value.

5. CONCLUSION

Experimental data complemented with a detailed atomistic KMC simulation study on B activation in pre-amorphized Si in such a way that EOR defects are far from the B profile have been presented. Under these conditions simulations show that B deactivation occurs through the interaction of thermally equilibrium Si interstitials with active B atoms, leading to the formation of

DOI: 10.1002/jnm

B_i pairs that are able to interact with pre-existing BICs. Moreover, the presence of a large amount of BICs in highly B-doped samples implies the introduction of relevant additional scattering centers. As a consequence, the value of R_S, and the device performance, is not only determined by the amount of electrically active B dose but also by the electrically inactive BICs. This result is relevant to optimize the B dose and annealing conditions for the fabrication of Si devices.

ACKNOWLEDGEMENTS

This work has been supported by the Spanish DGI under project TEC2008-06069.

REFERENCES

1. International Technology Roadmap for Semiconductors. Available at: http://public.itrs.net (2007 Edition).
2. Jain SC, Schoenmaker W, Lindsay R, Stolk PA, Decoutere S, Willander M, Maes HE. Transient enhanced diffusion of boron in Si. *Journal of Applied Physics* 2002; **91**(11):8919–8941.
3. Pelaz L, Jaraiz M, Gilmer GH, Gossmann HJ, Rafferty CS, Eaglesham DJ, Poate JM. B diffusion and clustering in ion implanted Si: the role of B cluster precursors. *Applied Physics Letters* 1997; **70**(17):2285–2287.
4. Aboy M, Pelaz L, Marques LA, Barbolla J, Mokhberi A, Takamura Y, Griffin PB, Plummer JD. Atomistic modeling of deactivation and reactivation mechanisms in high-concentration boron profiles. *Applied Physics Letters* 2003; **83**(20):4166–4168.
5. Armigliato A, Nobili D, Ostoja P, Servidori M, Solmi S. Solubility and precipitation of boron in silicon and supersaturation resulting by thermal predeposition. *Semiconductor Silicon 1977*; *The Electrochemical Society Softbound Proceedings Series* (*The Electrochemical Society*, *Pennington*, *NJ*) 1977; **77**(2):638–647.
6. Jin J-Y, Liu J, Jeong U, Mehta S, Jones K. Study of reverse annealing behaviors of p(+)/n ultrashallow junction formed using solid phase epitaxial annealing. *Journal of Vacuum Science and Technology B* 2002; **20**(1):422–426.
7. Lerch W, Paul S, Niess J, Cristiano F, Lamrani Y, Calvo P, Cherkashin N, Downey DF, Arevalo EA. Solid-phase-epitaxy—activation and deactivation of boron in ultra-shallow junctions. *Electrochemical Society Symposium Proceedings* 2004; **1**:90–105.
8. Mattoni A, Colombo L. Boron ripening during solid-phase epitaxy of amorphous silicon. *Physical Review B* 2004; **69**(4): Art. No. 045204.
9. Aboy M, Pelaz L, Marqués LA, López P, Barbolla J, Duffy R. Atomistic analysis of the evolution of boron activation during annealing in crystalline and preamorphized silicon. *Journal of Applied Physics* 2005; **97**(10): Art. No. 103520 (and references therein).
10. Aboy M, Pelaz L, López P, Marqués LA, Duffy R, Venezia VC. Physical insight into boron activation and redistribution during annealing after low-temperature solid phase epitaxial regrowth. *Applied Physics Letters* 2006; **88**(19): Art. No. 191917.
11. Aboy M, Pelaz L, López P, Bruno E, Mirabella S, Napolitani E. Evolution of boron-interstitial clusters in preamorphized silicon without the contribution of end-of-range defects. *Materials Science and Engineering B* 2008; **144–155**:247–251.
12. Masetti G, Severi M, Solmi S. Modeling of carrier mobility against carrier concentration in arsenic-doped, phosphorus-doped, and boron-doped silicon. *IEEE Transactions on Electronic Devices* 1983; **30**:764–769.
13. Law ME, Cea SM. Continuum based modeling of silicon integrated circuit processing: an object oriented approach. *Computational Materials Science* 1998; **12**(4):289–308.
14. Rafferty C, Smith RK. Making a PROPHET. *CMES-Computer Modeling in Engineering and Science* 2000; **1**(1):151–160.
15. Jaraiz M, Castrillo P, Pinacho R, Martín-Bragado I, Barbolla J. Atomistic front-end process modelling: a powerful tool for deep-submicron device fabrication. *Simulation of Semiconductor Processes and Devices* (*SISPAD*) *Proceedings*, Springer-Verlag Wien, Austria 2001; 10–17.
16. Blochl PE, Smargiassi E, Car R, Laks DG, Andreoni W, Pantelides ST. 1st-principles calculations of self-diffusion constants in silicon. *Physical Review Letters* 1993; **70**(16):2435–2438.
17. Jones RO, Gunnarsson O. The density functional formalism, its applications and prospects. *Review of Modern Physics* 1989; **61**(3):689–746.
18. Sadigh B, Lenosky TJ, Theiss SK, Caturla M-J, Diaz de la Rubia T, Foad MA. Mechanism of boron diffusion in silicon: an ab initio and kinetic Monte Carlo study. *Physical Review Letters* 1999; **83**(21):4341–4344.
19. Stillinger FH, Weber TA. Computer-simulation of local order in condensed phases of silicon. *Physical Review B* 1985; **31**(8):5262–5271.

DOI: 10.1002/jnm

20. Tersoff J. Empirical interatomic potential for silicon with improved elastic properties. *Physical Review B* 1988; **38**(14):9902–9905.
21. Marqués LA, Pelaz L, Castrillo P, Barbolla J. Molecular dynamics study of the configurational and energetic properties of the silicon self-interstitial. *Physical Review B* 2005; **71**(8): Art. No. 085204.
22. Gilmer GH, Diaz de la Rubia T, Stock DM, Jaraiz M. Diffusion and interactions of point-defects in silicon-molecular-dynamics simulations. *Nuclear Instruments and Methods in Physics Research B* 1995; **102**:247–255.
23. Marqués LA, Lourdes P, Maria A, Lourdes E, Juan B. Microscopic description of the irradiation-induced amorphization in silicon. *Physical Review Letters* 2003; **91**(13): Art. No. 135504.
24. Robinson MT, Torrens IM. Computer-simulation of atomic-displacement cascades in solids in binary-collision approximation. *Physical Review B* 1974; **9**(12):5008–5024.
25. Biersack JP, Haggmark LG. A Monte-Carlo computer-program for the transport of energetic ions in amorphous targets. *Nuclear Instruments and Methods* 1980; **174**:257–269.
26. Hernandez-Mangas JM, Arias J, Bailon L, Jaraiz M, Barbolla J. Improved binary collision approximation ion implant simulators. *Journal of Applied Physics* 2002; **91**(2):658–667.
27. Zhu J, Díaz de la Rubia T, Yang LH, Mailhiot C, Gilmer GH. Ab initio pseudopotential calculations of B diffusion and pairing in Si. *Physical Review B* 1996; **54**(7):4741–4747.
28. Windl W, Bunea MM, Stumpf R, Dunham ST, Masquelier MP. First-principles study of boron diffusion in silicon. *Physical Review Letters* 1999; **83**(21):4345–4348.
29. Liu XY, Windl W, Masquelier MP. Ab initio modeling of boron clustering in silicon. *Applied Physics Letters* 2000; **77**(13):2018–2020.
30. Lenosky TJ, Sadigh B, Theiss SK, Caturla MJ, Díaz de la Rubia T. Ab initio energetics of boron-interstitial clusters in crystalline Si. *Applied Physics Letters* 2000; **77**(12):1834–1836.
31. Bracht H, Haller EE, Clark-Phelps R. Silicon self-diffusion in isotope heterostructures. *Physical Review Letters* 1998; **81**(2):393–396.
32. Strobel M, La Magna A, Coffa S. A kinetic lattice Monte-Carlo approach to the evolution of boron in silicon. *Nuclear Instruments and Methods in Physics Research B* 2002; **186**:339–343.
33. Cowern NEB, Mannino G, Stolk PA, Roozeboom F, Huizing HGA, van Berkum JGM, de Boer WB, Cristiano F, Claverie A, Jaraiz M. Energetics of self-interstitial clusters in Si. *Physical Review Letters* 1999; **82**(22):4460–4463.
34. Eaglesham DJ, Stolk PA, Gossmann HJ, Poate JM. Implantation and transient B-diffusion in Si—the source of the interstitials. *Applied Physics Letters* 1994; **65**(18):2305–2307.
35. Cristiano F, Grisolia J, Colombeau B, Omri M, de Mauduit B, Claverie A, Giles LF, Cowern NEB. Formation energies and relative stability of perfect and faulted dislocation loops in silicon. *Journal of Applied Physics* 2000; **87**(12):8420–8428.
36. Rafferty CS, Gilmer GH, Jaraiz M, Eaglesham D, Gossmann H-J. Simulation of cluster evaporation and transient enhanced diffusion in silicon. *Applied Physics Letters* 1996; **68**(17):2395–2397.
37. Bongiorno A, Colombo L, Diaz De la Rubia T. Structural and binding properties of vacancy clusters in silicon. *Europhysics Letters* 1998; **43**(6):695–700.
38. Mirabella S, Bruno E, Priolo F, De Salvador D, Napolitani E, Drigo AV, Carnera A. Dissolution kinetics of boron-interstitial clusters in silicon. *Applied Physics Letters* 2003; **83**(4):680–682.
39. De Salvador D, Napolitani E, Bisognin G, Carnera A, Bruno E, Mirabella S, Impellizzeri G, Priolo F. Experimental evidences for two paths in the dissolution process of B clusters in crystalline Si. *Applied Physics Letters* 2005; **87**(22): Art. No. 221902.
40. Boninelli S, Mirabella S, Bruno E, Priolo F, Cristiano F, Claverie A, De Salvador D, Bisognin G, Napolitani E. Evolution of boron-interstitial clusters in crystalline Si studied by transmission electron microscopy. *Applied Physics Letters* 2007; **91**(3): Art. No. 031905.
41. Ziegler JF, Biersack JP, Littmark U. *The Stopping and Range of Ions in Solids*, *vol. 1 of Series Stopping and Ranges of Ions in Matter*, Pergamon Press, New York, 1984. www.srim.org.
42. Romano L, Napolitan E, Privitera V, Scalese S, Terrasi A, Mirabella S, Grimaldi MG. Carrier concentration and mobility in B doped $Si_{1x}Ge_x$. *Materials Science and Engineering B* 2003; **102**:49–52.
43. Pelaz L, Marqués LA, Aboy M, Barbolla J. Atomistic modeling of amorphization and recrystallization in silicon. *Applied Physics Letters* 2003; **82**(13):2038–2040.
44. Hobler G, Otto G. Status and open problems in modeling of as-implanted damage in silicon. *Materials Science in Semiconductor Processing* 2003; **6**:1–14.
45. Csepregi L, Kennedy EF, Mayer JW, Sigmon TW. Substrate-orientation dependence of epitaxial regrowth rate from Si-implanted amorphous Si. *Journal of Applied Physics* 1978; **49**(7):3906–3911.
46. Jain SH, Griffin PB, Plummer JD, McCoy S, Gelpey J, Selinger T, Downey DF. Metastable boron active concentrations in Si using flash assisted solid phase epitaxy. *Journal of Applied Physics* 2004; **96**(12):7357–7360.
47. Pelaz L, Marqués LA, Aboy M, López P, Barbolla J. Physical insight into ultra-shallow junction formation through atomistic modeling. *Nuclear Instruments and Methods in Physics Research B* 2005; **253**:41–45.
48. Boninelli S. Fondazione Istituto Italiano di Tecnologia (IIT), Via Morego 30, Genova, Italy, Private Communication, December 2008.

DOI: 10.1002/jnm

AUTHORS' BIOGRAPHIES

Maria Aboy was born in 1978 in Valladolid, Spain. She received the Master's Degree and her PhD in Physics at the University of Valladolid in 2001 and 2005, respectively. Her PhD thesis was related to dopant activation, dopant-defect interactions, and ultra-shallow junction formation. During her PhD study she spent several periods as a Visiting Research Fellow at IMEC, in Leuven, Belgium, working in collaboration with NXP (spin-off of Philips Semiconductors). In 2001 she also became a Junior Lecturer in the Department of Electronics at the University of Valladolid. She is co-author of about 35 publications on international scientific journals. Her current research interests include atomistic modeling and simulation of Si processes for nanometric devices.

Lourdes Pelaz received her MSc in Electronics Physics and her PhD from University of Valladolid, Spain, in 1991 and 1995, respectively. In 1996 she became a professor at University of Valladolid. From 1996 to 2000 she spent extensive periods of time at Bell Laboratories, Murray Hill, NJ, as visiting researcher. She is co-author of over 70 publications on international journals and holds one international patent. She has been invited to many international conferences and has co-organized four international scientific conferences. Her current research activities are related to atomistic modeling of front-end processes.

Pedro López received an MSc in Electronics Physics in 1998 from the University of Salamanca, Spain. He obtained the Electronic Engineer degree and his PhD from the University of Valladolid, Spain, in 2001 and 2009 respectively. Since 2004 he has worked as a Junior Lecturer at the University of Valladolid. He has also been a Visiting Research Fellow at IMEC, in Leuven, Belgium, working in collaboration with NXP (formerly Philips Semiconductor). His PhD thesis is related to the atomistic modeling of amorphization/recrystallization and impurity co-implantation processes for the fabrication of ultra-shallow junctions in Si. His current research interest focuses on the modeling of damage generation and amorphization induced by ion implantation in Ge.

Elena Bruno was born on 10 April 1978 in Catania (Italy). She attained her Master's Degree in Physics (110/110 summa cum laude) and her PhD in Materials Science at the University of Catania in 2003 and 2007, respectively. Since November 2006 she has had a post-doc position at the Center for Materials and Technologies for the Information and communication Science (MATIS) of the National Institute for the Physics of Matter (INFM) of CNR in Catania. Her research activity includes experimental studies of point-defects in crystalline silicon and germanium and their interaction and consequent effects on dopants behavior. She reported the research results in about 40 publications in international referred scientific journals, in 10 oral and 3 poster contributions in national and international conferences. She received 3 awards for her student and young researcher career. She took part in the Local Organizing Committee of the '15th International Conference on Ion Beam Modification of Materials (IBMM)'. Thanks to several scientific collaborations, she has interacted with many public and private Italian and foreign (both EU and USA) institutes.

DOI: 10.1002/jnm

Salvo Mirabella was born on 31 May 1976. He received his Laurea and PhD degrees in Physics from the University of Catania in 1999 and 2003, respectively. Since 2003 he joined the National Institute for the Physics of Matter (INFM), and he is now a member of the researcher staff of CNR-INFM MATIS. His research activity is mainly experimental, focusing on group IV advanced materials for Photovoltaics and Microelectronics (light absorption mechanisms in Si or Ge based nanostructures, sunlight-energy conversion, point-defects and dopants in crystalline silicon and germanium, ion beam modification of materials). He is co-author of about 90 publications on international scientific journals and of one international patent, co-worker of some EU and USA research institutes and universities. He has been invited as speaker at various international conferences and participant of several national and EU research projects. He co-organized two international scientific conferences (IBMM2006, E-MRS2009 Symposium I), being also co-Editor of the relative Proceeding Books, edited by Elsevier.

DOI: 10.1002/jnm